

AlignVAR: Towards Globally Consistent Visual Autoregression for Image Super-Resolution

Cencen Liu¹, Dongyang Zhang^{1,2}, Wen Yin¹, Jielei Wang^{1,2}, Tianyu Li¹,
 Ji Guo¹, Wenbo Jiang¹, Guoqing Wang¹, Guoming Lu^{1,2,*}

¹ University of Electronic Science and Technology of China

² Ubiquitous Intelligence and Trusted Services Key Laboratory of Sichuan Province

Abstract

Visual autoregressive (VAR) models have recently emerged as a promising alternative for image generation, offering stable training, non-iterative inference, and high-fidelity synthesis through next-scale prediction. This encourages the exploration of VAR for image super-resolution (ISR), yet its application remains underexplored and faces two critical challenges: **locality-biased attention**, which fragments spatial structures, and **residual-only supervision**, which accumulates errors across scales, severely compromises global consistency of reconstructed images. To address these issues, we propose **AlignVAR**, a globally consistent visual autoregressive framework tailored for ISR, featuring two key components: (1) Spatial Consistency Autoregression (SCA), which applies an adaptive mask to reweight attention toward structurally correlated regions, thereby mitigating excessive locality and enhancing long-range dependencies; and (2) Hierarchical Consistency Constraint (HCC), which augments residual learning with full reconstruction supervision at each scale, exposing accumulated deviations early and stabilizing the coarse-to-fine refinement process. Extensive experiments demonstrate that AlignVAR consistently enhances structural coherence and perceptual fidelity over existing generative methods, while delivering over 10× faster inference with nearly 50% fewer parameters than leading diffusion-based approaches, establishing a new paradigm for efficient ISR.

1. Introduction

Generative models, empowered by strong learned priors, have revolutionized the field of image super-resolution (ISR). Among them, Generative Adversarial Networks (GANs) [17, 19, 25] and Diffusion Models [23, 34, 45] have emerged as the two dominant paradigms. However, each of these approaches suffers from inherent limitations. GAN-based methods [17, 37, 48, 52], while enhancing perceptual

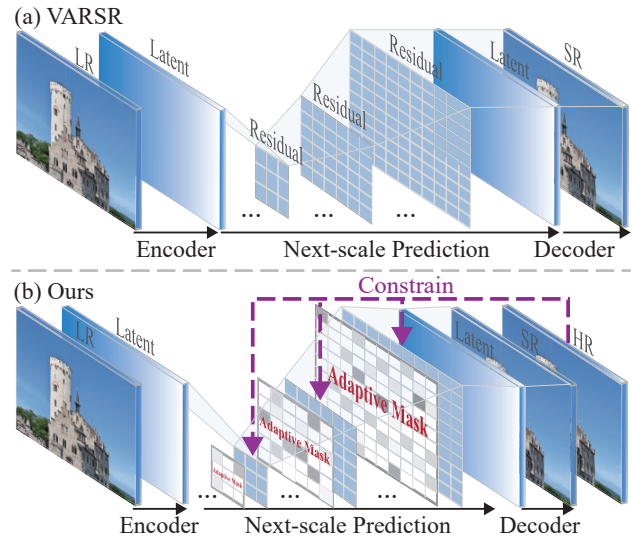


Figure 1. Comparison between the VARSR and AlignVAR. AlignVAR enhances VAR by introducing an adaptive consistency mask for intra-scale modeling and full reconstruction supervision for inter-scale alignment.

realism, often exhibit training instability and tend to introduce visually inconsistent artifacts [43]. Diffusion-based approaches [7, 23, 34, 43, 45] exploit powerful generative priors to achieve high-fidelity reconstruction, yet their iterative denoising process incurs heavy computational costs, substantially limiting their practicality [4].

These challenges have motivated the exploration of alternative generative paradigms for ISR, among which visual autoregressive (VAR) modeling has recently emerged as a promising direction [30, 41]. The coarse-to-fine prediction strategy of VAR naturally aligns with the hierarchical nature of ISR, which progressively restores image details across scales. The recent VARSR [27], as illustrated in Fig. 1, pioneers the application of VAR to ISR, demonstrating its initial feasibility. However, this seminal attempt also reveals a fundamental conflict: the model’s inherent locality bias and

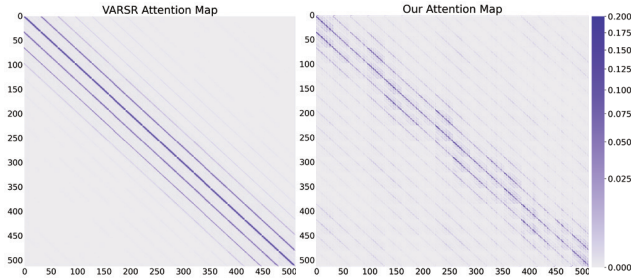


Figure 2. Comparison of attention distribution. Visualization of attention maps for VARSR and AlignVAR shows that VARSR exhibits highly localized attention concentrated in nearby regions, whereas AlignVAR captures broader contextual dependencies through the proposed Spatial Consistency Autoregression (SCA), thereby enhancing spatial coherence within each scale.

the cumulative error propagation across scales jointly undermine the global consistency required for ISR, resulting in degraded global coherence in the reconstructed images.

Building on this observation, we conduct a systematic analysis of the VARSR framework and identify two coupled root causes underlying its failure to maintain global consistency. The first is **Spatial Inconsistency**. The self-attention mechanism in VAR models exhibits a strong locality bias, with attention weights concentrated almost exclusively on adjacent regions, as illustrated in Fig. 2. This restricted receptive field limits the integration of global context, resulting in spatially disjoint artifacts such as fragmented textures and structural distortions, as shown in Fig. 3. The second is **Hierarchical Inconsistency**, which we analyze by injecting random perturbations into different scales and observing their influence on the final reconstruction, as shown in Fig. 4. These perturbations induce color shifts and structural misalignments, indicating that residual-only supervision allows small prediction errors from coarser scales to propagate and amplify through the hierarchy [15]. We argue that these issues stem from a common origin: the lack of explicit consistency constraints in both the intra-scale (spatial) and inter-scale (hierarchical) dimensions.

To address these limitations, we propose **AlignVAR**, a visual autoregressive framework designed to achieve globally consistent ISR. As shown in Fig. 1, AlignVAR introduces two complementary mechanisms that collaboratively promote coherence within and across scales by reweighting spatial attention and recalibrating hierarchical dependencies. Specifically, the *Spatial Consistency Autoregression (SCA)* adaptively reweights attention to emphasize structurally correlated regions rather than local neighborhoods, enabling the model to aggregate long-range context and maintain spatial continuity. Meanwhile, the *Hierarchical Consistency Constraint (HCC)* recalibrates cross-scale dependencies through a hierarchical supervision objective that enforces both residual and full-scale consistency between predictions and ground-truth representations. By allowing

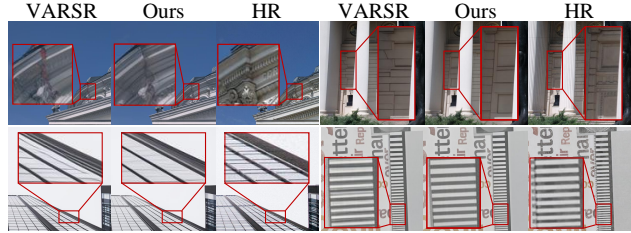


Figure 3. Spatial inconsistency results in texture discontinuities, structural distortions.

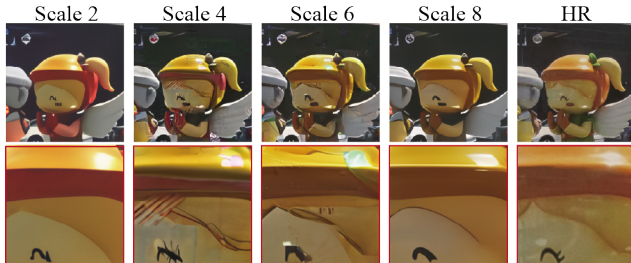


Figure 4. Hierarchical inconsistency results in color shifts and structural misalignment.

each scale to correct contextual deviations before they propagate, HCC effectively suppresses error accumulation and stabilizes refinement throughout the hierarchy. SCA and HCC form a unified consistency-driven autoregressive formulation that restores fine textures while preserving large-scale structural fidelity, yielding reconstructions that are both perceptually accurate and globally coherent.

In summary, we make the following key contributions:

- We revisit visual autoregression for ISR and identify two fundamental sources of inconsistency in existing VAR-based frameworks: *spatial inconsistency* arising from locality bias and *hierarchical inconsistency* caused by cumulative error propagation.
- We propose **AlignVAR**, a globally consistent VAR framework that enhances spatial coherence and hierarchical alignment through two complementary components: *Spatial Consistency Autoregression (SCA)* and *Hierarchical Consistency Constraint (HCC)*.
- Extensive experiments demonstrate that AlignVAR substantially improves reconstruction coherence and perceptual quality, establishing a strong benchmark for autoregressive real-world ISR.

2. Related Works

Image super-resolution. Early image super-resolution methods learn deterministic mappings from low-resolution to high-resolution images under simplified degradations such as bicubic downsampling, limiting their generalization to real-world scenarios [8, 10, 21, 22, 24, 53]. To overcome this, GAN-based approaches employ adversarial losses to approximate natural image distributions [16, 17, 37, 48, 52]. Methods like BSRGAN [49] and Real-ESRGAN [38] in-

roduce blind degradation modeling for robust real-world recovery, but often suffer from unstable training and unnatural artifacts [43]. Recently, diffusion-based SR methods such as DiffBIR [23], StableSR [34], SeeSR [43], PASD [45], and PiSA-SR [29] leverage generative priors from pre-trained diffusion models to enhance perceptual fidelity. Despite their strong visual performance, these models rely on iterative denoising, which incurs high computational cost and may produce hallucinated or inconsistent details [4, 26].

Visual autoregressive models. Autoregression, motivated by its success in large language models [1, 31], has recently gained traction in visual generation tasks. Most approaches discretize latent features using vector quantizers [18, 32] and predict tokens sequentially [6, 11, 39, 41, 46, 47]. However, next-token prediction over flattened sequences often breaks spatial structure, which makes it difficult to generate coherent high-resolution content [30]. Visual autoregressive modeling [30] addresses this limitation through next-scale prediction, reconstructing images progressively across multiple scales and achieving strong generative performance. This paradigm has also been explored in image restoration [36] and further extended to ISR through VARSR [27], which reconstructs HR images in a coarse-to-fine manner. Nevertheless, VARSR still suffers from locality bias and cumulative error propagation, leading to both spatial and hierarchical inconsistency.

3. Preliminaries

In next-scale visual autoregression, image reconstruction is performed hierarchically within the latent space of a vector-quantized variational autoencoder (VQ-VAE) [32]. At each scale k , the latent feature f_k is computed as the residual between the target latent f and the upsampled reconstructions from all previous coarser scales:

$$f_k = f - \sum_{m=1}^{k-1} \text{upsample}(\text{lookup}(\mathcal{V}, r_m)), \quad (1)$$

where \mathcal{V} denotes the shared codebook, and $\text{lookup}(\mathcal{V}, r_m)$ retrieves the embedded vectors corresponding to tokens r_m .

Each latent position is quantized to the nearest codebook entry, yielding the discrete token map r_k :

$$r_k(i, j) = \arg \min_{v \in [|\mathcal{V}|]} \|\text{lookup}(\mathcal{V}, v) - f_k(i, j)\|_2^2. \quad (2)$$

Across scales, the overall autoregressive process follows a coarse-to-fine factorization:

$$p(r_1, r_2, \dots, r_K) = \prod_{k=1}^K p_{\theta}(r_k | r_1, r_2, \dots, r_{k-1}, c), \quad (3)$$

where c represents the conditional latent derived from the low-resolution input.

4. Methods

4.1. Motivation and Empirical Observation

We analyze the spatial behavior of visual autoregression (VAR) in image super-resolution by visualizing its attention distribution. As shown in Fig. 2, VARSR [27] exhibits highly localized attention responses, where most attention mass is confined to narrow regions, revealing a strong *local bias*. This bias limits long-range contextual aggregation and weakens spatial correlations among distant yet related structures. These observations indicate that sequential tokenization and limited receptive field lead to a non-conservative spatial information flow, resulting in spatial inconsistency within each scale. This motivates our first question:

Q1: *How can we mitigate the local bias of VAR to achieve spatial consistency within each scale?*

Hierarchical inconsistency caused by error accumulation. Beyond spatial coherence, the hierarchical prediction process of VAR inherently suffers from cumulative prediction errors, as shown in Fig. 4. In the next-scale prediction paradigm, each latent r_k is estimated based on imperfect outputs from preceding scales $r_{1:k-1}$. Any deviation in coarse-scale predictions shifts the conditional distribution $p(r_k | r_{1:k-1})$, leading to a compounding effect in which errors are propagated and amplified across scales. We attribute this problem to residual-only supervision used in existing VAR frameworks, which leaves intermediate latent representations under-constrained and destabilizes the generative hierarchy. This motivates our second question:

Q2: *How can we recalibrate intermediate predictions to maintain hierarchical consistency across scales?*

4.2. Overview

Motivated by the two issues identified above, we propose **AlignVAR**, a globally consistent visual autoregressive framework for ISR. The overall architecture of AlignVAR is illustrated in Fig. 5. Briefly, AlignVAR is composed of two primary modules: Spatial Consistency Autoregression (SCA) and Hierarchical Consistency Constraint (HCC). The SCA expands the effective receptive field and applies a learnable structure-aware mask to mitigate local attention bias (§4.3), while the HCC enforces full-scale latent alignment to recalibrate intermediate predictions and suppress cumulative drift across scales (§4.4). Together, these designs enable AlignVAR to produce perceptually faithful and structurally coherent high-resolution reconstructions.

4.3. Spatial Consistency Autoregression (SCA)

The core idea of SCA is to enhance spatial coherence within the autoregressive process. Rather than relying on order-based attention with an inherently local bias, SCA introduces a structure-aware conditioning principle that reweights contextual dependencies.

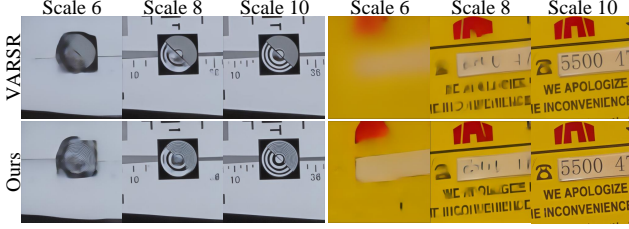


Figure 6. Comparison of multi-scale reconstructions. AlignVAR alleviates cumulative error propagation across scales and preserves more consistent structural and textural details than VARSR [27].

4.4. Hierarchical Consistency Constraint (HCC)

In the original next-scale autoregressive formulation, the Cross Entropy (CE) loss [30] supervises only the residual tokens predicted at each scale. While effective for local refinement, this residual-only supervision cannot correct errors accumulated from coarser levels, allowing scale-wise biases to propagate upward. To address this issue, we introduce HCC, which provides full-scale latent supervision to explicitly recalibrate hierarchical dependencies. By aligning predicted latent representations with their complete multi-scale ground truths, HCC enforces global consistency across the entire autoregressive hierarchy.

Full-scale representation. Given a high-resolution image $I_{HR} \in \mathbb{R}^{C \times H_K \times W_K}$, the VAE encoder \mathcal{E} produces its latent feature representation

$$z = \mathcal{E}(I_{HR}) \in \mathbb{R}^{C \times H_K \times W_K}. \quad (8)$$

To construct scale-specific ground truths for hierarchical supervision, we spatially downsample z to each target resolution S_k and quantize the result into discrete tokens:

$$u_{\text{gt}}^k = \mathcal{Q}(\text{Down}(z, S_k)), \quad S_k \in \{S_1, S_2, \dots, S_K\}, \quad (9)$$

where $\text{Down}(\cdot)$ denotes spatial downsampling to the resolution of scale k , and $\mathcal{Q}(\cdot)$ denotes the shared vector quantizer. Unlike the residual tokens used in the standard CE loss, u_{gt}^k represents the complete latent state at each scale, thus providing a stronger supervision target.

HCC loss. During autoregressive reconstruction, the model predicts residual tokens \hat{r}_{pred}^k for each scale. The corresponding cumulative (full-scale) latent prediction is obtained by aggregating residuals from all previous scales:

$$\hat{u}_{\text{pred}}^k = \hat{u}_{\text{pred}}^{k-1} + \hat{r}_{\text{pred}}^k, \quad \hat{u}_{\text{pred}}^{(0)} = \mathbf{0}. \quad (10)$$

We design the HCC loss to impose a multi-scale hierarchical alignment constraint between these cumulative predictions and the corresponding ground-truth latents:

$$\mathcal{L}_{\text{HCC}} = \sum_{k=1}^K \|\hat{u}_{\text{pred}}^k - u_{\text{gt}}^k\|_2^2. \quad (11)$$

This inter-scale calibration prevents error propagation and aligns the semantic content across the hierarchy.

By extending the supervision from residuals to full latent representations, the HCC loss bridges the semantic gap between hierarchical scales and stabilizes the coarse-to-fine refinement process. As shown in Fig. 6, AlignVAR reconstructs finer and more consistent textures at higher scales compared to VARSR [27], indicating that the proposed recalibration effectively alleviates the accumulation and propagation of local errors. Together with SCA’s spatial regularization, it establishes a unified mechanism that preserves intra-scale coherence and inter-scale consistency throughout the autoregressive super-resolution process.

4.5. Training Objective

Our training process is performed under the teacher-forcing paradigm [30], where the prediction at each scale is conditioned on the reweighted ground-truth tokens $\tilde{r}_{\text{gt}}^{1:k-1}$ and the low-resolution latent feature c , providing a stable and reliable supervision path throughout the entire multi-scale prediction procedure. The autoregressive predictor models a categorical distribution over the codebook entries at each spatial position (i, j) , optimized via a standard CE objective commonly used in modern generative modeling:

$$\mathcal{L}_{\text{CE}} = - \sum_{k=1}^K \sum_{(i,j)} \log p_{\theta}(r_{\text{gt}}^k(i, j) | \tilde{r}_{\text{gt}}^{1:k-1}, c). \quad (12)$$

Finally, the overall objective of AlignVAR combines both intra-scale and inter-scale learning signals, ensuring that each component contributes meaningfully to the reconstruction quality:

$$\mathcal{L}_{\text{total}} = \mathcal{L}_{\text{CE}} + \lambda \mathcal{L}_{\text{HCC}}, \quad (13)$$

where λ is a hyperparameter that balances the two components. Joint optimization of \mathcal{M}_{ϕ} and p_{θ} encourages spatially coherent predictions at each scale and hierarchically consistent dependencies across the reconstruction process, ultimately improving both stability and performance.

5. Experimental Results

5.1. Experimental Setups

Datasets. AlignVAR is trained on LSDIR [20] and the first 10K face images from FFHQ [13], where low-resolution counterparts are synthesized using the RealESRGAN degradation pipeline [38]. For evaluation, we adopt both synthetic and real-world benchmarks. The synthetic validation set (DIV2K-Val) is built by randomly cropping 3K patches from DIV2K [3], while real-world evaluation is conducted on DRealSR [42] and RealSR [35]. Following [30], all HR images are standardized to 512×512 and their LR inputs to 128×128 .

Table 1. Comparison with state-of-the-art methods on synthetic and real-world benchmarks. The best and second-best results are highlighted in **bold red** and underline blue, respectively.

Datasets	Metrics	GAN-based			Diffusion-based					VAR-based	
		BSRGAN	Real-ESR	SwinIR	LDM	StableSR	DiffBIR	PASD	UPSR	VARSR	AlignVAR
DIV2K-Val	PSNR↑	<u>24.42</u>	24.30	23.77	21.66	23.26	23.49	23.59	24.87	24.41	24.35
	SSIM↑	0.6164	0.6324	0.6186	0.4752	0.5670	0.5568	0.5899	<u>0.6294</u>	0.6189	0.6021
	LPIPS↓	0.3511	0.3267	0.3910	0.4887	0.3228	0.3638	0.3611	0.3173	<u>0.2985</u>	0.2955
	DISTS↓	0.2369	0.2245	0.2291	0.2693	0.2116	0.2177	0.2134	<u>0.2132</u>	0.2167	0.2162
	FID↓	50.99	44.34	44.45	55.04	28.32	34.55	39.74	39.48	<u>28.64</u>	25.71
	MANIQA↑	0.3547	0.3756	0.3411	0.3589	0.4173	<u>0.4598</u>	0.4440	0.3635	0.4137	0.4665
	CLIPQA↑	0.5253	0.5205	0.5213	0.5570	<u>0.6752</u>	0.6731	0.6573	0.5748	0.6312	0.6754
	MUSIQ↑	60.18	59.76	57.21	57.46	65.19	65.57	66.58	62.38	<u>66.88</u>	67.32
RealSR	PSNR↑	26.38	25.68	25.88	25.66	24.69	24.94	25.21	25.97	26.08	<u>26.11</u>
	SSIM↑	<u>0.7651</u>	0.7614	0.7671	0.6934	0.7090	0.6664	0.7140	0.7449	0.7381	0.7125
	LPIPS↓	<u>0.2656</u>	0.2710	0.2614	0.3367	0.3003	0.3485	0.2986	0.2862	0.2777	0.2871
	DISTS↓	0.2124	0.2060	<u>0.2061</u>	0.2324	0.2134	0.2257	0.2125	0.2083	0.2111	0.2123
	FID↓	141.25	135.14	132.80	133.34	131.72	<u>127.59</u>	139.42	140.11	118.84	138.81
	MANIQA↑	0.3763	0.3736	0.3561	0.3375	0.4167	0.4378	<u>0.4418</u>	0.3893	0.4316	0.4553
	CLIPQA↑	0.5114	0.4487	0.4433	0.6053	0.6200	<u>0.6396</u>	0.6009	0.5856	0.5953	0.6784
	MUSIQ↑	63.28	60.37	59.28	56.32	65.25	64.32	66.61	64.79	<u>66.65</u>	68.53
DRealSR	PSNR↑	28.70	28.61	28.20	27.78	27.87	26.57	27.45	29.21	<u>28.84</u>	28.54
	SSIM↑	<u>0.8028</u>	0.8052	0.7983	0.7152	0.7427	0.6516	0.7539	0.8018	0.7735	0.7682
	LPIPS↓	<u>0.2858</u>	0.2819	0.2830	0.3745	0.3333	0.4537	0.3331	0.2872	0.3102	0.3184
	DISTS↓	0.2144	<u>0.2089</u>	0.2103	0.2417	0.2297	0.2724	0.2322	0.2050	0.2311	0.2340
	FID↓	155.62	147.66	146.38	164.87	148.18	160.67	173.40	157.83	141.99	<u>145.44</u>
	MANIQA↑	0.3441	0.3435	0.3311	0.3342	0.3897	<u>0.4602</u>	0.4551	0.3339	0.4225	0.4685
	CLIPQA↑	0.5061	0.4525	0.4522	0.5984	0.6321	<u>0.6445</u>	0.6365	0.5537	0.6395	0.6534
	MUSIQ↑	57.16	54.27	53.01	51.37	58.72	61.06	<u>63.69</u>	55.88	62.66	63.83

Implementation details. AlignVAR is trained using a scale-wise autoregressive transformer backbone consisting of 24 transformer blocks. The model is initialized from pre-trained VAR weights [30] for faster convergence. Training uses AdamW [2] with a batch size of 32, weight decay of 5×10^{-2} , and an initial learning rate of 5×10^{-5} decayed via cosine annealing. The model is optimized for 100 epochs, with the loss balancing coefficient λ in Eq. 13 set to 1.0. All experiments are conducted on 8 NVIDIA H100 GPUs.

Evaluation metrics. To comprehensively evaluate both fidelity and perceptual quality, we adopt a diverse set of reference-based and no-reference metrics. For fidelity, PSNR and SSIM [40] are computed on the Y channel of the YCbCr color space. Perceptual similarity is measured using LPIPS [51] and DISTS [9], while distributional alignment is assessed with FID [12]. We further employ no-reference metrics, including MANIQA [44], MUSIQ [14], and CLIPQA [33], to evaluate visual naturalness.

Compared models. We compare AlignVAR with state-of-the-art (SOTA) methods in two categories. The first includes GAN-based methods: BSRGAN [49], Real-ESRGAN [38], and SwinIR-GAN [21]. The second covers diffusion-based methods: LDM [28], StableSR [34], DiffBIR [23], PASD [45], and UPSR [50]. We also include the recent autoregressive method VARSR [27], retrained on our dataset for fairness. Other competing models are evaluated using official implementations and pretrained weights.

5.2. Comparison with SOTA

Quantitative comparisons. As shown in Table 1, AlignVAR performs strongly across both synthetic and real-world benchmarks, substantially improving overall perceptual quality. On the DIV2K-Val dataset, it outperforms GAN-based and diffusion-based methods in all perceptual metrics, achieving the lowest FID of 25.71 and the best LPIPS of 0.2955 among all compared models. On RealSR, AlignVAR significantly increases MUSIQ from 66.65 to 68.53 and CLIPQA from 0.5953 to 0.6784 compared to VARSR [27], demonstrating its consistent effectiveness. Although AlignVAR does not achieve the highest fidelity metrics, this is expected because fine details in LR images are severely degraded and cannot be fully recovered by any existing method. AlignVAR consistently produces high-quality super-resolution results that better align with human visual perception, offering perceptually realistic, visually coherent, and structurally consistent reconstructions.

Qualitative comparisons. Fig. 7 presents visual comparisons with representative ISR methods. Some artifacts highlight common shortcomings of existing paradigms: GAN-based models often cause local distortions and jagged edges, while diffusion-based models may hallucinate textures and weaken structural alignment. In contrast, AlignVAR reconstructs sharp edges, coherent textures, and natural color transitions, better aligning with human visual perception. Notably, when true high-frequency details are ir-

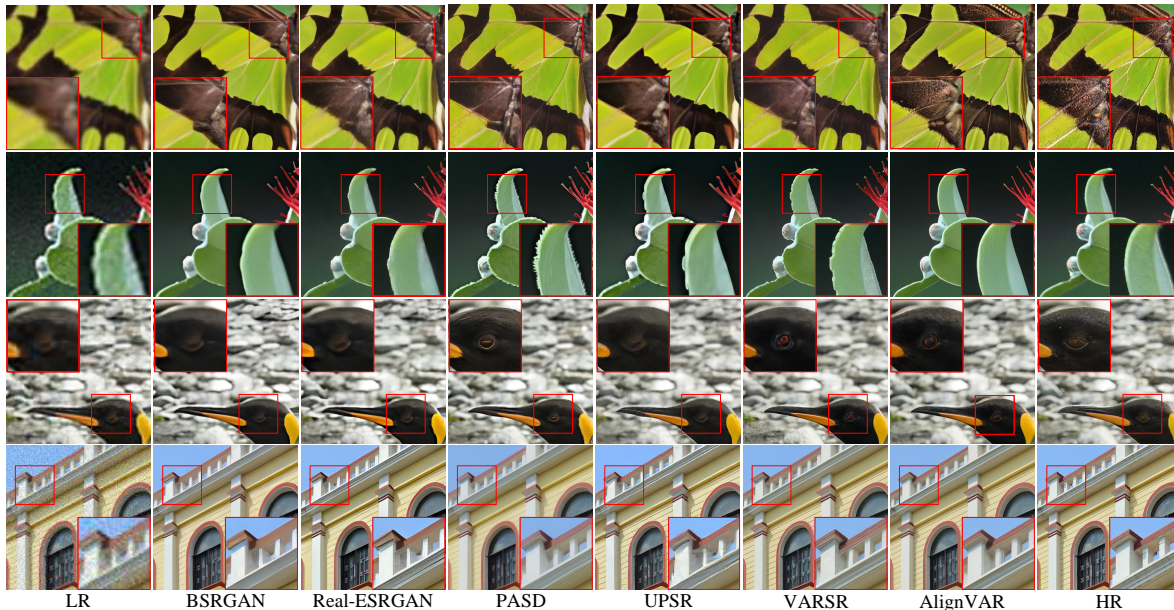


Figure 7. Qualitative comparisons with representative methods.

Table 2. Complexity comparison.

Models	Params	Steps	Inference Time
StableSR	1409.1M	200	15.32s
DiffBIR	1900.4M	20	5.03s
PASD	1716.7M	50	5.94s
UPSR	1530.9M	5	2.79s
VARSR	1102.9M	10	0.52s
AlignVAR	1056.5M	10	0.43s

Table 3. Ablation study of the SCA. “w/o” denotes removing SCA, “RI” indicates random input, and “SG” represents the structural guidance used in our model.

Metrics	RealSR			DrealSR		
	w/o SCA	RI	SG	w/o SCA	RI	SG
PSNR \uparrow	26.77	26.67	26.11	29.32	28.68	28.54
LPIPS \downarrow	0.2847	0.2855	0.2871	0.2975	0.3077	0.3184
DISTS \downarrow	0.2079	0.2108	0.2123	0.2253	0.2289	0.2340
MANIQA \uparrow	0.4351	0.4435	0.4553	0.4285	0.4312	0.4685
MUSIQ \uparrow	66.74	67.21	68.53	62.75	63.06	63.83

recoverably lost in the low-resolution input, AlignVAR preserves the recoverable structures and generates perceptually plausible textures. This explains its clearly superior no-reference metric scores, even if the reference metric scores in Table 1 are not correspondingly higher.

Complexity comparisons. As shown in Table 2, AlignVAR achieves significantly higher efficiency than diffusion-based models and VARSR [27]. Diffusion-based methods require iterative refinement, leading to long inference times even with a limited number of sampling steps. In contrast, AlignVAR reconstructs a 512×512 image in only 0.43 seconds, which is over $10\times$ faster than PASD and more than $5\times$ faster than the 5-step UPSR. This efficiency stems from the scale-wise prediction strategy, where early scales in-

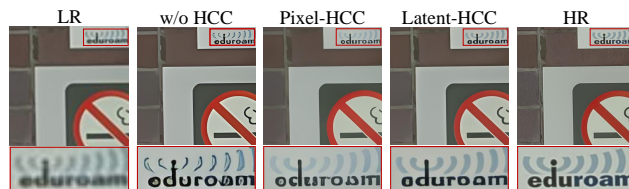


Figure 8. Comparison of supervision domains for HCC.

volve fewer tokens and thus incur lower computational cost. Compared with the autoregressive baseline VARSR, which incorporates an additional diffusion refiner at the expense of increased parameters and latency, AlignVAR removes this component and adopts a lightweight mask generator that introduces negligible overhead. Thus, AlignVAR achieves better overall performance with fewer parameters and faster inference. Further analysis of the efficiency advantage of AlignVAR is provided in the Supplementary Material.

5.3. Ablation Study and Analysis

Effectiveness of SCA. We evaluate the effectiveness of SCA on the RealSR and DRealSR datasets, as shown in Table 3. Three configurations are compared: removing SCA, using random input for the mask generator (RI), and applying the proposed structural guidance (SG). Removing SCA slightly improves fidelity metrics but noticeably degrades perceptual scores, while random input leads to unstable textures and weakened visual coherence. These results demonstrate that SCA effectively exploits structural guidance to enhance spatial consistency and achieves a better balance between fidelity and perceptual quality.

Effectiveness of HCC. We evaluate the impact of HCC on the RealSR and DRealSR datasets, as shown in Ta-

Table 4. Ablation on the Hierarchical Consistency Constraint.

Metrics	RealSR		DrealSR	
	w/o HCC	HCC	w/o HCC	HCC
PSNR \uparrow	25.85	26.11	28.23	28.54
LPIPS \downarrow	0.2898	0.2871	0.3208	0.3184
DISTS \downarrow	0.2175	0.2123	0.2411	0.2340
MANIQA \uparrow	0.4431	0.4553	0.4442	0.4685
MUSIQ \uparrow	67.06	68.53	62.85	63.83

Table 5. Effect of the balancing coefficient λ on RealSR.

Settings	PSNR \uparrow	LPIPS \downarrow	DISTS \downarrow	MANIQA \uparrow	MUSIQ \uparrow
$\lambda = 0.5$	25.83	0.2874	0.2184	0.4403	67.56
$\lambda = 1.0$	26.11	0.2871	0.2123	0.4553	68.53
$\lambda = 1.5$	26.21	0.2785	0.2107	0.4465	67.85
$\lambda = 2.0$	26.35	0.2703	0.2079	0.4337	67.03

ble 4. Introducing HCC consistently improves both fidelity and perceptual metrics, indicating that aligning full-scale latent representations strengthens cross-scale information flow and stabilizes hierarchical prediction. We further compare applying this constraint in latent space versus in pixel space and observe that latent space supervision achieves noticeably better perceptual coherence, as illustrated in Fig. 8. Overall, HCC effectively suppresses accumulated errors and enhances inter-scale consistency, yielding reconstructions that are both more accurate and visually coherent.

Influence of the balancing coefficient. We study the effect of the balancing coefficient λ in Eq. 13 on the RealSR dataset, as shown in Table 5. When λ increases from 0.5 to 1.0, both perceptual and fidelity metrics improve, with the best perceptual quality achieved at $\lambda = 1.0$. Further increasing λ beyond 1.0 slightly enhances distortion-oriented scores but leads to a decrease in perceptual quality. These results suggest that $\lambda = 1.0$ provides better overall performance in terms of perceptual quality while maintaining competitive fidelity scores.

Analysis of the Adaptive Mask. Fig. 9 visualizes the structural guidance, the corresponding initial and learned masks, and the reweighted feature map. The structural guidance captures coarse edges and contours, which are transferred to the initial mask as a spatial bias. After training, the learned mask becomes sharper and more selective, concentrating on semantic boundaries such as windmill blades and Chinese characters while suppressing activations in smooth background regions. The reweighted feature map highlights these structural areas with clearer and more coherent responses, suggesting that the mask adaptively emphasizes perceptually important regions. Overall, this process enables more structure-aware feature interaction and improves spatial consistency in the reconstructed images.

Analysis of HCC. To further understand the effect of HCC, we analyze its impact on hierarchical recalibration and robustness to perturbations. Fig. 10 (left) plots the mean

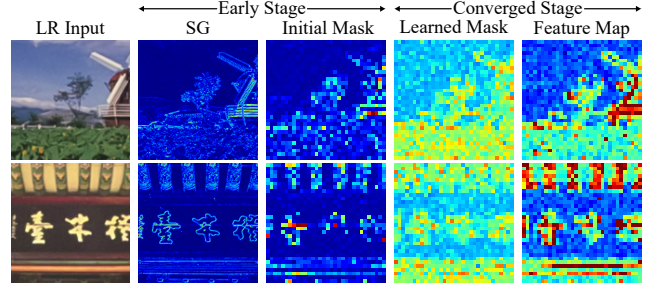


Figure 9. Analysis of the adaptive mask at different training stages. SG denotes the structural guidance extracted from the LR input.

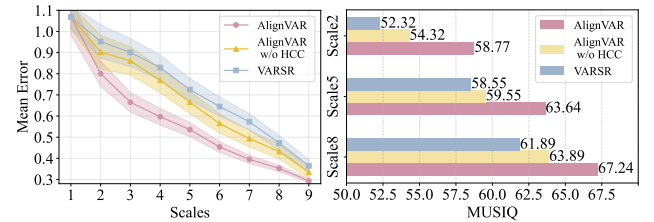


Figure 10. Quantitative analysis of the Hierarchical Consistency Constraint on RealSR. Shown are the mean prediction errors across scales (left) and the MUSIQ scores under identical random perturbations injected at different scales (right).

squared error (MSE) at each prediction scale. AlignVAR without HCC already reduces overall errors compared with VARSR, and adding HCC further lowers the MSE at early and middle scales, indicating that HCC serves as a coarse-to-fine recalibration mechanism that corrects global structures before finer refinement. For robustness evaluation, we inject identical random perturbations into latent features at scales 2, 5, and 8 and report MUSIQ scores in Fig. 10 (right). AlignVAR shows the smallest MUSIQ degradation under all noise levels, confirming that HCC improves inter-scale stability against cumulative perturbations.

6. Conclusion

We present **AlignVAR**, a globally consistent visual autoregressive framework for image super-resolution. Through a detailed and comprehensive technical analysis of inconsistency issues in existing VAR models, we identify spatial local bias and hierarchical error propagation as the main bottlenecks severely hindering coherent and accurate reconstruction. To alleviate these issues, we introduce Spatial Consistency Autoregression to adaptively reweight fine-grained intra-scale attention and Hierarchical Consistency Constraint to recalibrate multi-level inter-scale dependencies through joint residual and full-scale supervision. Extensive experiments on both synthetic and real-world benchmarks consistently demonstrate that AlignVAR achieves an excellent overall balance between fidelity and perceptual quality. This work provides a new perspective for achieving globally coherent and reliable visual autoregression for high-quality image super-resolution.

References

- [1] Josh Achiam, Steven Adler, Sandhini Agarwal, Lama Ahmad, Ilge Akkaya, Florencia Leoni Aleman, Diogo Almeida, Janko Altenschmidt, Sam Altman, Shyamal Anadkat, et al. Gpt-4 technical report. *arXiv preprint arXiv:2303.08774*, 2023. 3
- [2] Kingma DP Ba J Adam et al. A method for stochastic optimization. *arXiv preprint arXiv:1412.6980*, 1412(6), 2014. 6
- [3] Eirikur Agustsson and Radu Timofte. Ntire 2017 challenge on single image super-resolution: Dataset and study. In *CVPR workshops*, pages 126–135, 2017. 5
- [4] Sumukh K Aithal, Pratyush Maini, Zachary Lipton, and J Zico Kolter. Understanding hallucinations in diffusion models through mode interpolation. *NeurIPS*, 37:134614–134644, 2024. 1, 3
- [5] Peter J Burt and Edward H Adelson. The laplacian pyramid as a compact image code. In *Readings in computer vision*, pages 671–679. Elsevier, 1987. 4
- [6] Huiwen Chang, Han Zhang, Lu Jiang, Ce Liu, and William T Freeman. Maskgit: Masked generative image transformer. In *CVPR*, pages 11315–11325, 2022. 3
- [7] Bin Chen, Gehui Li, Rongyuan Wu, Xindong Zhang, Jie Chen, Jian Zhang, and Lei Zhang. Adversarial diffusion compression for real-world image super-resolution. In *Proceedings of the Computer Vision and Pattern Recognition Conference*, pages 28208–28220, 2025. 1
- [8] Xiangyu Chen, Xintao Wang, Jiantao Zhou, Yu Qiao, and Chao Dong. Activating more pixels in image super-resolution transformer. In *Proceedings of the IEEE/CVF conference on computer vision and pattern recognition*, pages 22367–22377, 2023. 2
- [9] Keyan Ding, Kede Ma, Shiqi Wang, and Eero P Simoncelli. Image quality assessment: Unifying structure and texture similarity. *IEEE transactions on pattern analysis and machine intelligence*, 44(5):2567–2581, 2020. 6
- [10] Chao Dong, Chen Change Loy, Kaiming He, and Xiaoou Tang. Learning a deep convolutional network for image super-resolution. In *European conference on computer vision*, pages 184–199. Springer, 2014. 2
- [11] Baisong Guo, Xiaoyun Zhang, Haoning Wu, Yu Wang, Ya Zhang, and Yan-Feng Wang. Lar-sr: A local autoregressive model for image super-resolution. In *2022 IEEE/CVF Conference on Computer Vision and Pattern Recognition (CVPR)*, pages 1899–1908, 2022. 3
- [12] Martin Heusel, Hubert Ramsauer, Thomas Unterthiner, Bernhard Nessler, and Sepp Hochreiter. Gans trained by a two time-scale update rule converge to a local nash equilibrium. *NeurIPS*, 30, 2017. 6
- [13] Tero Karras, Samuli Laine, and Timo Aila. A style-based generator architecture for generative adversarial networks. In *Proceedings of the IEEE/CVF conference on computer vision and pattern recognition*, pages 4401–4410, 2019. 5
- [14] Junjie Ke, Qifei Wang, Yilin Wang, Peyman Milanfar, and Feng Yang. Musiq: Multi-scale image quality transformer. In *ICCV*, pages 5128–5137, 2021. 6
- [15] Hermann Kumbong, Xian Liu, Tsung-Yi Lin, Ming-Yu Liu, Xihui Liu, Ziwei Liu, Daniel Y Fu, Christopher Re, and David W Romero. Hmar: Efficient hierarchical masked autoregressive image generation. In *CVPR*, pages 2535–2544, 2025. 2
- [16] Wei-Sheng Lai, Jia-Bin Huang, Narendra Ahuja, and Ming-Hsuan Yang. Deep laplacian pyramid networks for fast and accurate super-resolution. In *CVPR*, pages 624–632, 2017. 2
- [17] Christian Ledig, Lucas Theis, Ferenc Huszár, Jose Caballero, Andrew P. Aitken, Alykhan Tejani, Johannes Totz, Zehan Wang, and Wenzhe Shi. Photo-realistic single image super-resolution using a generative adversarial network. *2017 IEEE Conference on Computer Vision and Pattern Recognition (CVPR)*, pages 105–114, 2016. 1, 2
- [18] Doyup Lee, Chiheon Kim, Saehoon Kim, Minsu Cho, and Wook-Shin Han. Autoregressive image generation using residual quantization. In *CVPR*, pages 11523–11532, 2022. 3
- [19] Wenbo Li, Kun Zhou, Lu Qi, Liying Lu, and Jiangbo Lu. Best-buddy gans for highly detailed image super-resolution. In *Proceedings of the AAAI Conference on Artificial Intelligence*, pages 1412–1420, 2022. 1
- [20] Yawei Li, Kai Zhang, Jingyun Liang, Jiezhang Cao, Ce Liu, Rui Gong, Yulun Zhang, Hao Tang, Yun Liu, Denis Demandolx, et al. Lsdir: A large scale dataset for image restoration. In *Proceedings of the IEEE/CVF Conference on Computer Vision and Pattern Recognition*, pages 1775–1787, 2023. 5
- [21] Jingyun Liang, Jiezhang Cao, Guolei Sun, Kai Zhang, Luc Van Gool, and Radu Timofte. Swinir: Image restoration using swin transformer. In *ICCV*, pages 1833–1844, 2021. 2, 6
- [22] Bee Lim, Sanghyun Son, Heewon Kim, Seungjun Nah, and Kyoung Mu Lee. Enhanced deep residual networks for single image super-resolution. In *Proceedings of the IEEE conference on computer vision and pattern recognition workshops*, pages 136–144, 2017. 2
- [23] Xinqi Lin, Jingwen He, Ziyan Chen, Zhaoyang Lyu, Bo Dai, Fanghua Yu, Yu Qiao, Wanli Ouyang, and Chao Dong. Diffbir: Toward blind image restoration with generative diffusion prior. In *ECCV*, pages 430–448. Springer, 2024. 1, 3, 6
- [24] Cencen Liu, Dongyang Zhang, Guoming Lu, Wen Yin, Jielei Wang, and Guangchun Luo. Srmamba-t: Exploring the hybrid mamba-transformer network for single image super-resolution. *Neurocomput.*, 624(C), 2025. 2
- [25] Chenxi Ma. Uncertainty-aware gan for single image super resolution. In *Proceedings of the AAAI Conference on Artificial Intelligence*, pages 4071–4079, 2024. 1
- [26] Supreeth Narasimhaswamy, Uttaran Bhattacharya, Xiang Chen, Ishita Dasgupta, Saayan Mitra, and Minh Hoai. Handiffuser: Text-to-image generation with realistic hand appearances. In *CVPR*, pages 2468–2479, 2024. 3
- [27] Yunpeng Qu, Kun Yuan, Jinhua Hao, Kai Zhao, Qizhi Xie, Ming Sun, and Chao Zhou. Visual autoregressive modeling for image super-resolution. In *ICML*, 2025. 1, 3, 5, 6, 7
- [28] Robin Rombach, Andreas Blattmann, Dominik Lorenz, Patrick Esser, and Björn Ommer. High-resolution image synthesis with latent diffusion models. In *CVPR*, pages 10684–10695, 2022. 6

- [29] Lingchen Sun, Rongyuan Wu, Zhiyuan Ma, Shuaizheng Liu, Qiaosi Yi, and Lei Zhang. Pixel-level and semantic-level adjustable super-resolution: A dual-lora approach. In *Proceedings of the Computer Vision and Pattern Recognition Conference*, pages 2333–2343, 2025. 3
- [30] Keyu Tian, Yi Jiang, Zehuan Yuan, Bingyue Peng, and Liwei Wang. Visual autoregressive modeling: Scalable image generation via next-scale prediction. *NeurIPS*, 37:84839–84865, 2024. 1, 3, 5, 6
- [31] Hugo Touvron, Thibaut Lavril, Gautier Izacard, Xavier Martinet, Marie-Anne Lachaux, Timothée Lacroix, Baptiste Rozière, Naman Goyal, Eric Hambro, Faisal Azhar, et al. Llama: Open and efficient foundation language models. *arXiv preprint arXiv:2302.13971*, 2023. 3
- [32] Aaron Van Den Oord, Oriol Vinyals, et al. Neural discrete representation learning. *NeurIPS*, 30, 2017. 3
- [33] Jie Wang, Yixin Li, Yifan Wang, Siyuan Chen, Qifan Wang, and Zhangyang Wang. Clip-iqa: No-reference image quality assessment with contrastive pre-training. In *CVPR*, pages 1502–1511, 2023. 6
- [34] Jianyi Wang, Zongsheng Yue, Shangchen Zhou, Kelvin CK Chan, and Chen Change Loy. Exploiting diffusion prior for real-world image super-resolution. *International Journal of Computer Vision*, 132(12):5929–5949, 2024. 1, 3, 6
- [35] Jianyi Wang, Zongsheng Yue, Shangchen Zhou, Kelvin CK Chan, and Chen Change Loy. Exploiting diffusion prior for real-world image super-resolution. *International Journal of Computer Vision*, 132(12):5929–5949, 2024. 5
- [36] Siyang Wang and Feng Zhao. Varformer: Adapting var’s generative prior for image restoration. *arXiv e-prints*, pages arXiv–2412, 2024. 3
- [37] Xintao Wang, Ke Yu, Shixiang Wu, Jinjin Gu, Yihao Liu, Chao Dong, Yu Qiao, and Chen Change Loy. Esrgan: Enhanced super-resolution generative adversarial networks. In *Proceedings of the European conference on computer vision (ECCV) workshops*, pages 0–0, 2018. 1, 2
- [38] Xintao Wang, Liangbin Xie, Chao Dong, and Ying Shan. Real-esrgan: Training real-world blind super-resolution with pure synthetic data. In *ICCV*, pages 1905–1914, 2021. 2, 5, 6
- [39] Xinlong Wang, Xiaosong Zhang, Zhengxiong Luo, Quan Sun, Yufeng Cui, Jinsheng Wang, Fan Zhang, Yueze Wang, Zhen Li, Qiyang Yu, et al. Emu3: Next-token prediction is all you need. *arXiv preprint arXiv:2409.18869*, 2024. 3
- [40] Zhou Wang, Alan C Bovik, Hamid R Sheikh, and Eero P Simoncelli. Image quality assessment: from error visibility to structural similarity. *IEEE transactions on image processing*, 13(4):600–612, 2004. 6
- [41] Hongyang Wei, Shuaizheng Liu, Chun Yuan, and Lei Zhang. Perceive, understand and restore: Real-world image super-resolution with autoregressive multimodal generative models. *arXiv preprint arXiv:2503.11073*, 2025. 1, 3
- [42] Pengxu Wei, Ziwei Xie, Hannan Lu, Zongyuan Zhan, Qixiang Ye, Wangmeng Zuo, and Liang Lin. Component divide-and-conquer for real-world image super-resolution. In *ECCV*, pages 101–117. Springer, 2020. 5
- [43] Rongyuan Wu, Tao Yang, Lingchen Sun, Zhengqiang Zhang, Shuai Li, and Lei Zhang. Seers: Towards semantics-aware real-world image super-resolution. In *CVPR*, pages 25456–25467, 2024. 1, 3
- [44] Sidi Yang, Tianhe Wu, Shuwei Shi, Han Gong, Jing Cao, Bin Yang, Xu Jia, and Xiaogang Zhu. Maniqa: Multi-dimension attention network for no-reference image quality assessment. In *CVPR*, pages 1191–1200, 2022. 6
- [45] Tao Yang, Rongyuan Wu, Peiran Ren, Xuansong Xie, and Lei Zhang. Pixel-aware stable diffusion for realistic image super-resolution and personalized stylization. In *ECCV*, pages 74–91. Springer, 2024. 1, 3, 6
- [46] Jiahui Yu, Yuanzhong Xu, Jing Yu Koh, Thang Luong, Gunjan Baid, Zirui Wang, Vijay Vasudevan, Alexander Ku, Yinfei Yang, Burcu Karagol Ayan, et al. Scaling autoregressive models for content-rich text-to-image generation. *arXiv preprint arXiv:2206.10789*, 2(3):5, 2022. 3
- [47] Kaiwen Yu, Qi He, Gang Wu, and Zhijin Qin. Partial sampling-based semantic communications. *IEEE Transactions on Communications*, 73(10):9059–9070, 2025. 3
- [48] Yuan Yuan, Siyuan Liu, Jiawei Zhang, Yongbing Zhang, Chao Dong, and Liang Lin. Unsupervised image super-resolution using cycle-in-cycle generative adversarial networks. In *Proceedings of the IEEE conference on computer vision and pattern recognition workshops*, pages 701–710, 2018. 1, 2
- [49] Kai Zhang, Jingyun Liang, Luc Van Gool, and Radu Timofte. Designing a practical degradation model for deep blind image super-resolution. In *ICCV*, pages 4791–4800, 2021. 2, 6
- [50] Leheng Zhang, Weiyi You, Kexuan Shi, and Shuhang Gu. Uncertainty-guided perturbation for image super-resolution diffusion model. In *CVPR*, pages 17980–17989, 2025. 6
- [51] Richard Zhang, Phillip Isola, Alexei A. Efros, Eli Shechtman, and Oliver Wang. The unreasonable effectiveness of deep features as a perceptual metric. In *2018 IEEE/CVF Conference on Computer Vision and Pattern Recognition (CVPR)*, pages 586–595, 2018. 6
- [52] Wenlong Zhang, Yihao Liu, Chao Dong, and Yu Qiao. Ranksrgan: Generative adversarial networks with ranker for image super-resolution. In *Proceedings of the IEEE/CVF international conference on computer vision*, pages 3096–3105, 2019. 1, 2
- [53] Yulun Zhang, Kunpeng Li, Kai Li, Lichen Wang, Bineng Zhong, and Yun Fu. Image super-resolution using very deep residual channel attention networks. In *Proceedings of the European conference on computer vision (ECCV)*, pages 286–301, 2018. 2